

A Role for Two-Pore Channel Type 2 (TPC2)-Mediated Regulation of Membrane Contact Sites During Zebrafish Notochord Biogenesis?

Contact
Volume 6: 1–17
© The Author(s) 2023
Article reuse guidelines:
sagepub.com/journals-permissions
DOI: 10.1177/25152564231211409
journals.sagepub.com/home/ctc



Keira L. Rice^{1,#}, Ching Man Chan^{1,#}, Jeffrey J. Kelu^{1,§},
Andrew L. Miller¹, and Sarah E. Webb¹ 

Abstract

We have previously shown that in the developing trunk of zebrafish embryos, two-pore channel type 2 (TPC2)-mediated Ca²⁺ release from endolysosomes plays a role in the formation of the skeletal slow muscle. In addition, TPC2-mediated Ca²⁺ signaling is required for axon extension and the establishment of synchronized activity in the primary motor neurons. Here, we report that TPC2 might also play a role in the development of the notochord of zebrafish embryos. For example, when *tpcn2* was knocked down or out, increased numbers of small vacuoles were formed in the inner notochord cells, compared with the single large vacuole in the notochord of control embryos. This abnormal vacuolation was associated with embryos displaying attenuated body axis straightening. We also showed that TPC2 has a distinct pattern of localization in the notochord in embryos at ~24 hpf. Finally, we conducted RNAseq to identify differentially expressed genes in *tpcn2* mutants compared to wild-type controls, and found that those involved in actin filament severing, cellular component morphogenesis, Ca²⁺ binding, and structural constituent of cytoskeleton were downregulated in the mutants. Together, our data suggest that TPC2 activity plays a key role in notochord biogenesis in zebrafish embryos.

Keywords

notochord development, endolysosomal vesicles, two-pore channel type 2, *tpcn2* mutants and morphants, *trans-Ned19*, zebrafish embryos

Introduction

The notochord is a defining feature of members of the Chordata phylum. It lies ventral to the neural tube and is regarded as a form of primitive cartilage, acting initially as the main structural support of the body for most vertebrates (Stemple, 2005). In mammals and bony fish, the notochord is a transient structure, existing only in the embryonic and larval stages before being replaced by cartilage and bone in the adult (Hejnal and Lowe, 2014). However, some notochordal cells persist as they contribute to the nucleus pulposus, which lies between the intervertebral discs of the spinal cord (McCann et al., 2012; McCann and Séguin, 2016). In addition to its supportive role, the notochord also helps to coordinate development via the secretion of morphogens (Corallo et al., 2015), which diffuse into and specify the cells that form the adjacent tissues, such as the dorsal aorta, floor plate, and slow-twitch skeletal muscle (Baressi et al., 2000; Cleaver et al., 2000; Stemple, 2005).

In zebrafish, the notochord arises from the embryonic shield. At ~16.5 h post fertilization (hpf), chordamesoderm cells differentiate via a Notch-dependent mechanism into two cell types. These are outer epithelial sheath cells,

which secrete a thick perinotochordal extracellular matrix (ECM) and inner vacuolated cells, which contain large vacuoles and smaller pre-vacuolar compartments. Indeed, when mature, the inner vacuolated cells are characterized by large (~40 μm in diameter) fluid-filled vacuoles that occupy ~80% of the cell volume (Hunter et al., 2007; Yamamoto et al., 2010), and have a “stack of coins” appearance along the length of the

¹The Division of Life Science and Key State Laboratory for Molecular Neuroscience, HKUST, Hong Kong, People's Republic of China

Received June 27, 2023. Revised October 9, 2023. Accepted October 16, 2023.

[#]Joint first author.

[§]Present address: Randall Centre of Cell and Molecular Biophysics, Faculty of Life Sciences and Medicine, Guy's Campus, King's College London, London, UK.

Corresponding Author:

Sarah E. Webb, The Division of Life Science and Key State Laboratory for Molecular Neuroscience, HKUST, Clear Water Bay, Hong Kong, People's Republic of China.
Email: barnie@ust.hk



notochord (Glickman et al., 2003; Ellis et al., 2013a). These notochord features mediate trunk straightening and axis elongation by acting as a hydrostatic skeleton for the developing embryonic trunk before the bony skeleton forms (Bagnat and Gray, 2020; Bagwell et al., 2020).

During notochord development in zebrafish, relatively small intracellular pre-vacuoles become fused to form a single main vacuole in each internal notochord cell (Bagwell et al., 2020). Vacuolar inflation is driven by osmolyte transport into the vacuole lumen, creating turgor within the mechanically restrictive boundaries of the surrounding sheath cells. Notochord vacuoles are proposed to be lysosome-related organelles, and their formation requires the Golgi apparatus as well as endolysosomal trafficking and targeting machinery (Ellis et al., 2013a). It has been suggested that the pre-vacuoles bear a resemblance to “vacuolinos,” a recently discovered type of organelle in plants, which fuse to the tonoplast, a semipermeable membrane surrounding the main plant cell vacuole (Li et al., 2021). The fusion of the notochord pre-vacuoles therefore represents a key membrane contact event during notochord biogenesis (Vassileva et al., 2020).

In some zebrafish mutants (e.g., *dstyk*), the notochord is malformed. Disrupting *dstyk* expression was shown to prevent vesicle membrane fusion to (and thus the formation of) the main vacuoles, and this was associated with the notochord abnormalities observed (Bagwell et al., 2020). A separate study showed that there is an accumulation of Rab7a-puncta in the notochord of *dysk* mutant embryos, indicating defects in the late-endosome trafficking pathway (Sun et al., 2020). The same group provided evidence that *Dstyk* might exert transcriptional regulation on late endosomal trafficking and notochord vacuole biogenesis via the mTORC1/TFEB pathway (Sun et al., 2020). Early studies also highlighted a role for intracellular trafficking-related proteins in the formation of the perinotochordal basement membrane of the notochord. For example, Coutinho et al. (2004) showed that the *sneezy*, *happy*, and *dopey* zebrafish mutants fail to form inflated notochord vacuoles.

Accumulating evidence also suggests that an array of lysosomal ion channels (including TPCs and members of the Transient Receptor Potential cation channel, MucoLipin subfamily; TRPML) and transporters regulate membrane contact events. They achieve this by sensing trafficking and osmotic cues, which result in ion, solute, and water influx, as well as localized secretory events (Dong et al., 2010; Kilpatrick et al., 2013; Vassileva et al., 2020; Hu et al., 2022), all of which might be required for notochord biogenesis (Coutinho et al., 2004). Furthermore, various recent studies suggest that many trafficking associated genes are required to develop and maintain the characteristic stiffness and architecture of the notochord (Bagnat and Gray, 2020; Yasuoka, 2020).

As endolysosomal trafficking has been increasingly implicated in the formation of the notochord (Coutinho et al., 2004), we investigated the possible role of two-pore channel type 2 (TPC2) in this process. TPCs are pleiotropic cation-permeable channels found in endolysosomal

membranes, which are integral to intracellular Ca^{2+} signaling (Kilpatrick et al., 2017; Jin et al., 2020; Vassileva et al., 2020) and other transmembrane ion fluxes including Na^{+} , which might contribute to osmotically driven vacuole inflation (Wang et al., 2012; Cang et al., 2013; Vassileva et al., 2020). TPCs have been implicated in multiple cellular processes such as cell growth, differentiation, and development (Webb et al., 2020), cardiac dysfunction (Capel et al., 2015; Davidson et al., 2015), autophagy (Lin et al., 2015), and viral infection (Sakurai et al., 2015; Gunaratne et al., 2018). TPC2 is one of the three TPC isoforms present in most vertebrates, and it is expressed primarily in the membranes of lysosomes and late endosomes (Ruas et al., 2014). Numerous recent reports suggest that the genetic ablation or pharmacological inhibition of TPC2 results in distinctly abnormal developmental phenotypes, which include the disruption of skeletal muscle myogenesis (Kelu et al., 2015, 2017); inhibition of primary motor neuron extension (Guo et al., 2020), and abnormal pigmentation (Ambrosio et al., 2016). Such abnormal phenotypes likely arise via the disruption of key cellular processes including endolysosomal vesicle trafficking (Grimm et al., 2017); autophagy (Lin et al., 2015; García-Rúa et al., 2016; Vassileva et al., 2020) and/or key membrane contact events that include endocytosis and exocytosis (Davis et al., 2012, 2020), in a variety of cell types, tissues, and organs.

Here, we used a combinatorial approach, by applying genetic, molecular, pharmacological, and various live and fixed-imaging techniques, to explore the possible Ca^{2+} -related role of TPC2 in the formation of the notochord in zebrafish embryos. In addition, immunohistochemistry was used to determine the localization of TPC2 in the notochord of embryos at ~24 hpf. We also conducted RNAseq to identify genes that were upregulated or downregulated in *tpcn2* mutants compared with wild-type controls. Here, we propose that TPC2 functions to regulate key membrane contact events resulting in vacuole inflation in the inner notochord cells. Thus, our new data add notochord biogenesis as another key developmental event by which TPC2 plays an important regulatory role. This supports the growing recognition that one function of TPCs might be to act as master orchestrators of intracellular vesicle trafficking via Ca^{2+} -mediated regulation of membrane contact events. Indeed, their location in the membranes of highly motile Ca^{2+} stores provides the potential for highly localized signaling activity within differentiating cells (Marchant and Patel, 2015; Grimm et al., 2017; Kilpatrick et al., 2017; Vassileva et al., 2020).

Results

Genetic Attenuation of *tpcn2* has Distinct Effects on the Notochord at ~24 hpf

We previously demonstrated that the genetic attenuation of *tpcn2* has distinct effects on the development of the slow muscle cells in the trunk of zebrafish embryos (Kelu et al., 2015, 2017). Here, we observed that *tpcn2* knockout or

knockdown also had distinct effects on the development of the notochord. As shown in the low magnification images in Figure 1A–F and the bar chart in Figure 1G, embryos injected with *tpcn2*-T-MO (plus *p53*-MO) and *tpcn2* heterozygous (*tpcn2*^{+/-}) and homozygous (*tpcn2*^{-/-}) mutants, all exhibited significantly delayed body axis straightening when compared with the controls (i.e., the untreated, standard control (SC)-MO or *p53*-MO injected embryos) at ~24 hpf. The *tpcn2*-T-MO was co-injected with a *p53*-MO to prevent possible off-target effects of the former on p53 activity (Robu et al., 2007).

The gross morphology of the notochord vacuoles of the inner notochord cells was observed at higher magnification (Figure 2). Figure 2Aa shows a low magnification view of a wild-type embryo and the location on the trunk (black rectangle) where the notochord was imaged at higher magnification, whereas Figure 2B shows a schematic of the basic structures of the notochord and surrounding tissues. The bright-field images acquired at higher magnification (Figure 2Ca–d) show that in wild-type (ABTU strain) embryos (Figure 2Ca), the notochord cells could be identified by their large, fluid-filled vacuoles, whereas *tpcn2*^{-/-} mutant embryos contained a larger number of smaller notochord vacuoles (Figure 2Cb). In addition, wild-type embryos that were injected with the *p53*-MO displayed a comparable phenotype to that of the ABTU embryos (compare Figure 2Cc with Figure 2Ca), whereas embryos that were injected with the *tpcn2*-T-MO (plus *p53*-MO) exhibited a notochord vacuole phenotype similar to the *tpcn2*^{-/-} mutants (compare Figure 2Ad with Figure 2Cb).

The number and shape (i.e., circularity) of the notochord vacuoles were quantified for all the treatment groups (Figure 2D). Regarding the former, the number of vacuoles within a notochord region of interest (ROI) adjacent to somites 8–11 was quantified (Figure 2Da). The data show that the *tpcn2*^{-/-} mutants and morphants had significantly more vacuoles in this region than their respective controls (i.e., the ABTU and *p53*-MO-injected embryos). Regarding the shape (Figure 2Db), the data show that the *tpcn2* mutants and morphants possessed significantly more circular notochord vacuoles when compared with their respective controls.

To further quantify the notochord vacuole phenotype, embryos were labeled with BODIPY FL C₅-ceramide (Figure 3A). As this dye labels the Golgi apparatus within the cell cytoplasm (Chazotte, 2008), it was used to facilitate the identification (and quantification of the size) of the notochord vacuoles in the different wild-type and mutant lines, as well as in the various MO knockdown and pharmacological treatment groups. Quantification of BODIPY FL C₅-ceramide-labeled images in each of the treatment groups showed that injection of the *tpcn2*-T-MO (plus *p53*-MO) led to a significantly reduced vacuole area, when compared with the *p53*-MO controls (compare Figure 3Ad with Figure 3Ac, and Figure 3B). In addition, the area of the vacuoles in the *tpcn2*^{-/-} mutant was also significantly

smaller than those of wild-type (ABTU) embryos (compare Figure 3Af with Figure 3Ae, and Figure 3B). Embryos were also pharmacologically treated with *trans*-Ned-19, a selective inhibitor of NAADP-induced Ca²⁺ release (Pitt et al., 2010; Ruas et al., 2010), to investigate the possible involvement of Ca²⁺-mediated regulation of notochord development. Our data show that even though the DMSO solvent control had an effect on notochord vacuole size when compared with the untreated controls, embryos treated with *trans*-Ned-19 (and DMSO) had significantly smaller notochord vacuoles when compared with the DMSO-treated control embryos (compare Figure 3Ah with Figure 3Ag and see Figure 3B).

TPC2 is Localized to Distinct Regions in the Zebrafish Notochord at ~24 hpf

To study the localization of TPC2 in the zebrafish notochord at ~24 hpf, intact embryos were immunolabeled with an anti-TPC2 antibody and then counterstained with phalloidin and Hoechst 33258 to label the F-actin and nuclei, respectively (Figure 4). Confocal single optical sections were acquired through the notochord along the anterior–posterior axis of the zebrafish trunk adjacent to the location of somites 8 (Figure 4A), 16 (Figure 4B), and 22 (Figure 4C). Our data showed that the anti-TPC2 antibody displayed some nuclear labeling in the notochord cells in the anterior part of the notochord (yellow arrowheads in Figure 4Aa–Ac). TPC2 was also localized in distinct puncta, which were associated with the vacuolated notochord cell boundaries in the anterior, middle, and posterior regions of the notochord (white arrowheads in Figure 4Ab,Ac,Bb,Bc,Cb,Cc). Together, these data suggest that TPC2 is expressed in distinct regions of the zebrafish notochord at ~24 hpf.

*RNA-seq Analysis of *tpcn2* Homozygous Mutants and Wild-Type (ABTU) Embryos*

To explore the genetic landscape of *tpcn2* mutants and identify candidate genes implicated in notochord development, a whole-transcriptome RNA-seq analysis was performed on samples collected from the trunk of *tpcn2* homozygous embryos or wild-type (ABTU) embryos at ~17 hpf, by which time the anterior chordamesoderm cells have differentiated into notochord vacuolated cells and are beginning to inflate (Ellis et al., 2013a).

A principal components analysis showed that the *tpcn2* homozygotes formed a distinct cluster that was separate from the wild-type controls (Figure 5A). Principal component 1 (PC1) explains 83% of the total variance and separates the mutants from the wild-type samples, whereas PC2 explains 7% of the total variance. This indicates that most of the variation in the transcriptomes was caused by the different genetic backgrounds of the samples.

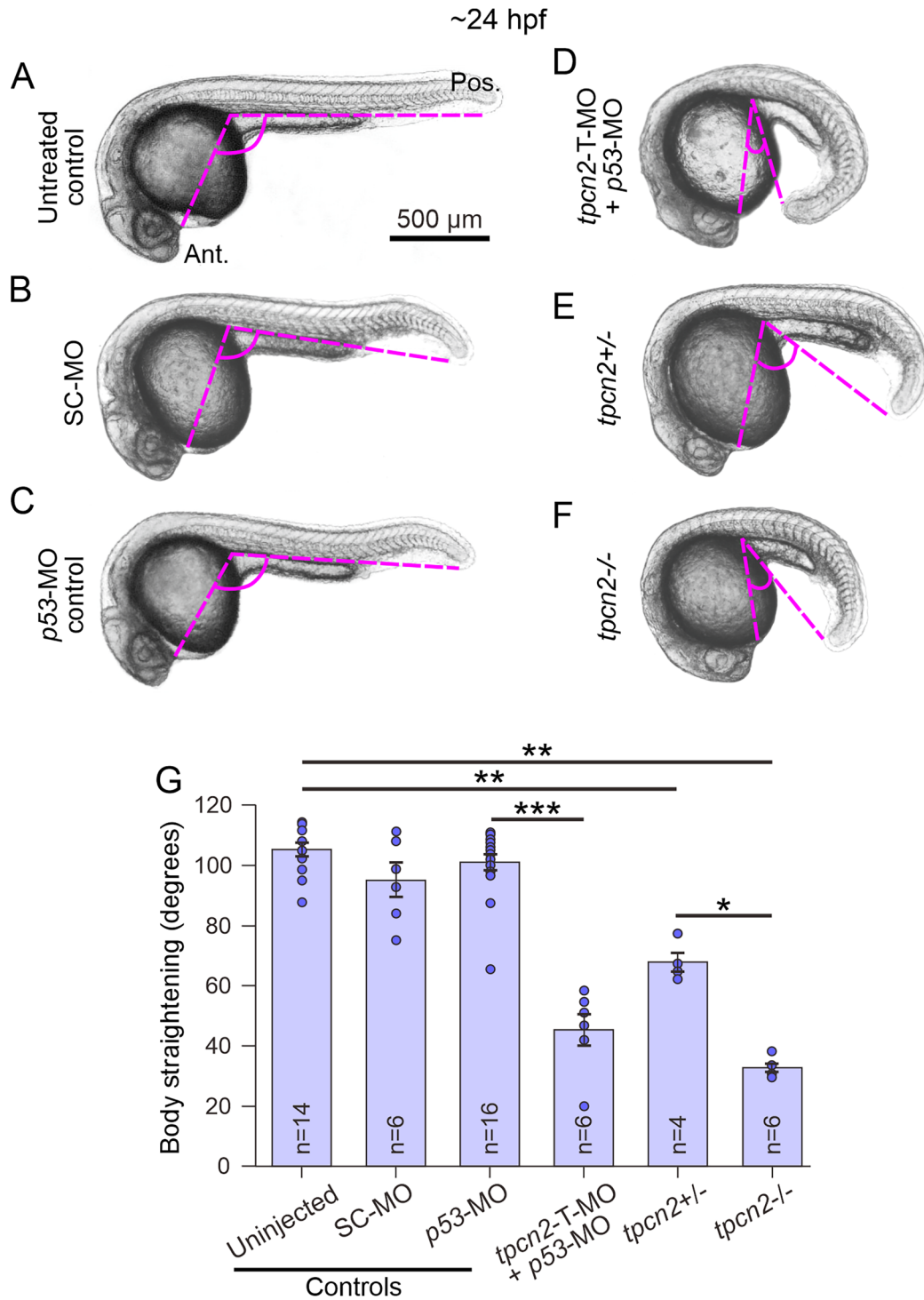


Figure 1. Effect of genetic attenuation of *tpcn2* on body axis straightening in embryos at ~24 hpf. Representative bright-field images showing the body axis straightening morphology in embryos at ~24–25 hpf. Embryos were (A) untreated (control) or injected with (B) standard control (SC)-MO, (C) p53-MO, or (D) *tpcn2*-MO-T + p53-MO. In addition, representative bright-field images of a (E) *tpcn2* heterozygous (*tpcn2*^{+/-}) and (F) *tpcn2* homozygous (*tpcn2*^{-/-}) mutant are shown. The body axis straightening angle (indicated by the pink dashed lines) was measured. Ant and Pos are anterior and posterior, respectively. Scale bar, 500 μ m. (G) Quantification of the body straightening angle. The bar chart shows the mean \pm SEM body straightening angle on to which is superimposed the individual data points. The number (*n*) of embryos in each condition is shown. Statistical analysis was carried out using the Mann–Whitney U-test and data that were significantly different are represented by **p* < .05, ***p* < .01, and ****p* < .001.

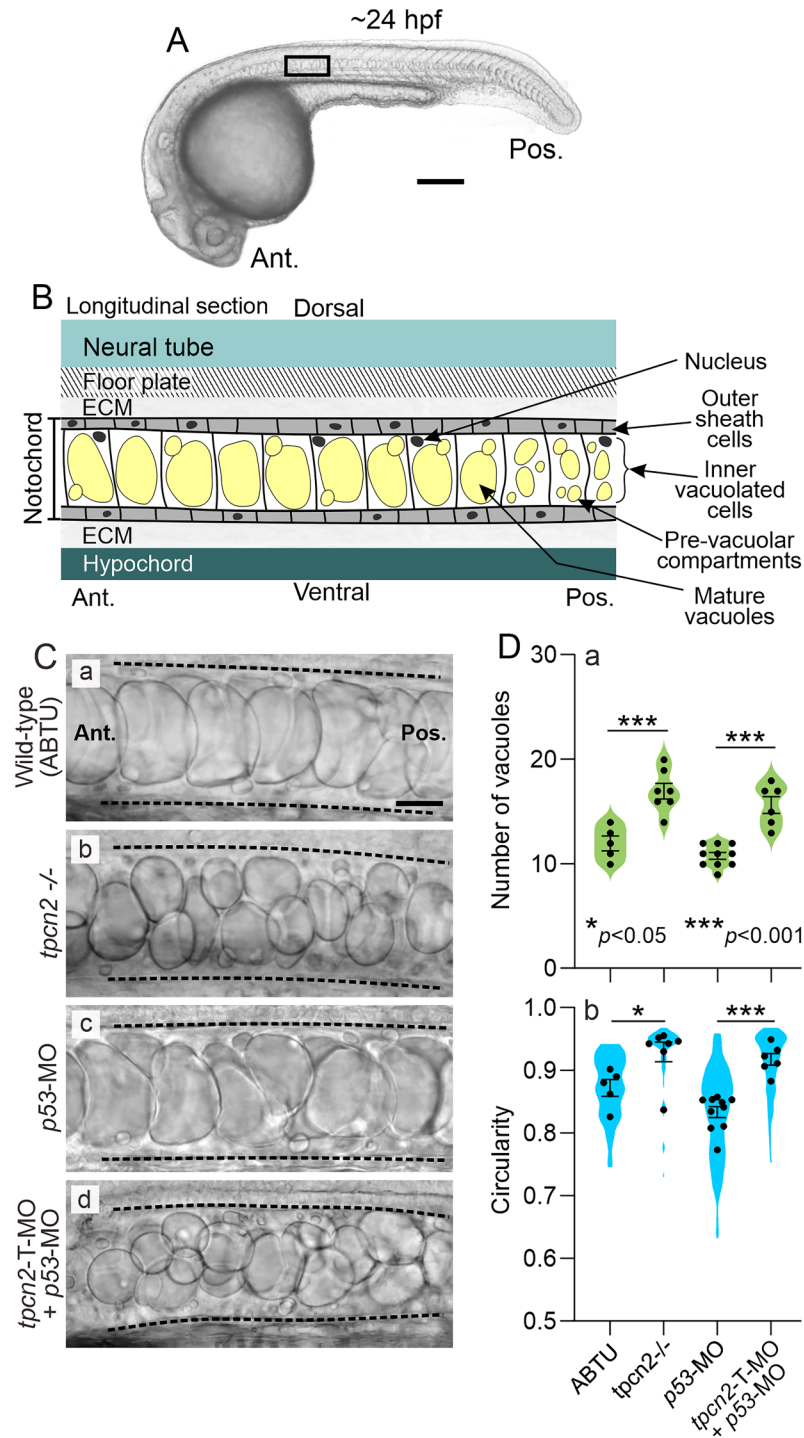


Figure 2. Effect of genetic attenuation of *tpcn2* on the number and shape of notochord vacuoles in embryos at ~24 hpf. **(A)** Bright-field image of an intact wild-type zebrafish embryo at ~24 hpf and **(B)** schematic showing the basic structure of the notochord from a lateral view. In **(A)**, the black rectangle indicates the location of the notochord (adjacent to somites 8–11), where higher magnification images were acquired. **(Ca-d)** Representative bright-field images showing lateral views of the notochord at higher magnification in a **(Ca)** wild-type (ABTU; $n = 5$) embryo, **(Cb)** *tpcn2* homozygous mutant (*tpcn2*^{-/-}; $n = 7$), **(Cc)** *p53*-MO-injected embryo ($n = 6$) and **(Cd)** *tpcn2*-T-MO + *p53*-MO-injected embryo ($n = 6$). In these images the black dashed lines indicate the dorsal and ventral boundaries of the notochord. Scale bars, 200 μm **(A)** and 20 μm **(C)**. **(D)** Violin-plots (indicating the mean \pm SEM) onto which are superimposed individual data points showing the **(Da)** number and **(Db)** circularity of the control, morphant, and mutant embryos shown in **(C)**. An explanation of what these parameters refer to is provided in the Experimental Procedures. The data were compared using one-way ANOVA and Fisher's least significant difference (LSD). Significance is indicated as * $p < .05$, and *** $p < .001$.

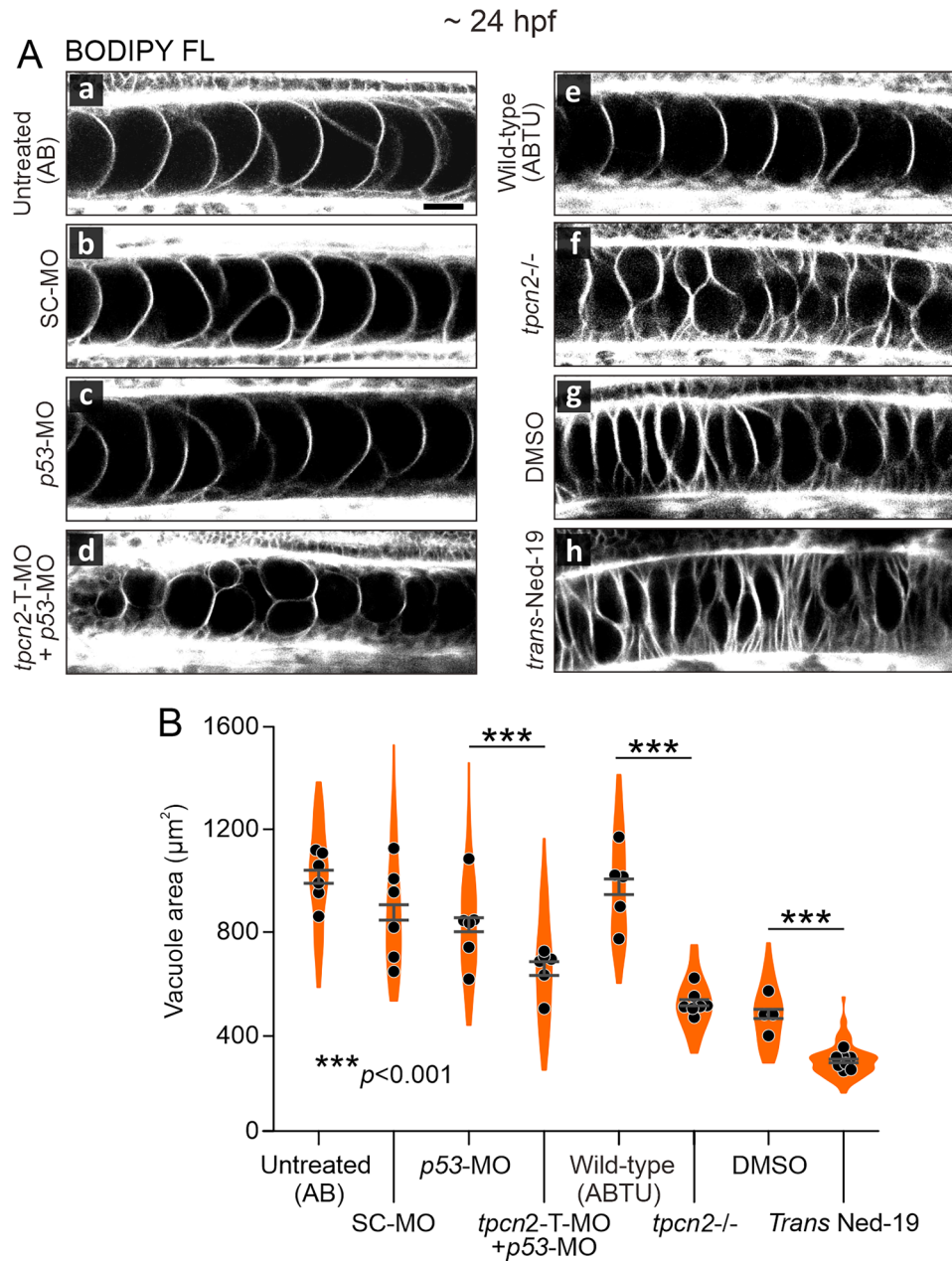


Figure 3. Effect of genetic attenuation of *tpcn2* or pharmacological inhibition of TPC2 on the size of the inner notochord cell main vacuole area in embryos at ~24 hpf **(A)** Representative confocal images showing lateral views of notochord vacuoles of **(Aa)** an uninjected wild-type (AB) embryo ($n=6$), and embryos injected with **(Ab)** standard control (SC)-MO ($n=6$); **(Ac)** p53-MO ($n=6$); or **(Ad)** *tpcn2*-T-MO + p53-MO ($n=6$). The notochord cell vacuoles of **(Ae)** wild-type (ABTU) embryos ($n=5$) and **(Af)** *tpcn2* homozygous mutants (*tpcn2*^{-/-}; $n=7$); as well as embryos treated with **(Ag)** DMSO ($n=4$) or **(Ah)** *trans*-Ned-19 ($n=8$) are also shown. Scale bar, 20 µm. **(B)** Violin-plot (indicating mean \pm SEM) onto which individual data points are superimposed, showing the vacuole area (an explanation of what this parameter refers to is provided in the Experimental Procedures) in the control, morphant, mutant and pharmacological treated embryos shown in **(A)**. The data were compared using one-way ANOVA and Fisher's least significant difference (LSD). Significance is indicated as *** $p < 0.001$.

Differential expression (DE) gene analysis was performed to better compare the transcriptomic landscape of the *tpcn2* mutants with respect to the wild-type controls. The efficacy of *tpcn2* knockout in the *tpcn2* mutant line was previously demonstrated by RT-PCR

(Kelu et al., 2017) and RT-qPCR (Guo et al., 2020). These results were mirrored by the RNA-seq results, where the *tpcn2* transcripts were significantly downregulated in the *tpcn2* homozygous embryos compared to the wild-type controls (Figure 5B).

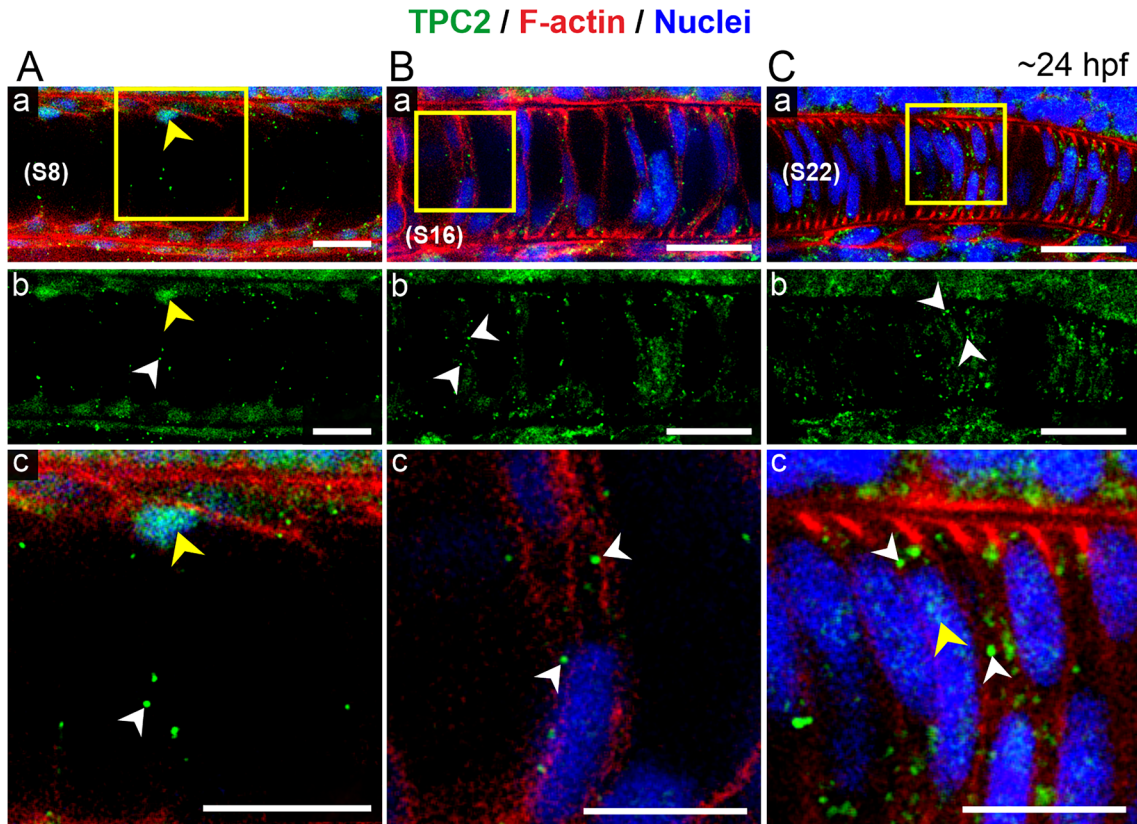


Figure 4. Localization of TPC2 in the notochord of intact embryos at ~24 hpf. Representative confocal images of the notochord in embryos ($n = 5$) immunolabeled with an anti-TPC2 antibody (green), and then counterstained with phalloidin (red) and Hoechst 33258 (blue), to visualize F-actin and the nuclei, respectively. These are single optical sections taken at the position of somite (S) **(A)** 8, **(B)** 16 and **(C)** 22. In **(Aa,Ac,Ba,Bc,Ca,Cc)**, the green, red and blue channels are merged, whereas in **(Ab,Bb,Cb)**, only the green channel (TPC2) is shown. **(Ac,Bc,Cc)** High magnification images of the regions bounded by the yellow square and rectangles in **(Aa,Ba,Ca)**. TPC2 puncta associated with the vacuolated notochord cells and nuclei are indicated by white and yellow arrowheads, respectively. Scale bars, 20 μm **(Aa,Ab,Ba,Bb,Ca,Cb)**, 10 μm **(Ac,Bc,Cc)**.

Among the 14,005 genes identified by RNA-seq, 858 (6.1%) genes were downregulated, and 785 (5.6%) genes were upregulated (with a cut-off of $p < .05$ and $|\text{fold-change}| > 1.5$). The top five genes with the most significantly altered expression include: *actin-depolymerizing factor/gelsolin* (*gsnb*), which is a key regulator of actin filament assembly and disassembly (Sun et al., 1999); *annexin A1b* (*anxa1b*), which is a Ca^{2+} -dependent phospholipid binding protein (Raynal and Pollard, 1994); *phosphatidylinositol glycan anchor biosynthesis class P* (*pigp*), which is involved in glycosylphosphatidylinositol (GPI)-anchor biosynthesis (Kinoshita and Fujita, 2016); *thymocyte nuclear protein 1* (*thyn1*), which is a poorly characterized nuclear protein believed to be involved in apoptosis (Miyaji et al., 2002), and *methylthioribulose-1-phosphate dehydratase* (*apip*), which is an enzyme involved in the methionine salvage pathway (Mary et al., 2012). The top 10 most significantly changed genes are highlighted in Figure 5C and the full list of differentially expressed genes (DEGs) have been deposited in NCBI's Gene Expression Omnibus (Edgar et al.,

2002) and are accessible through GEO Series accession number GSE229162 (<https://www.ncbi.nlm.nih.gov/geo/query/acc.cgi?acc=GSE229162>).

The top 50 DEGs that passed the statistical cut-off in the *tpcn2*^{-/-} mutants compared to the wild-type embryos were visualized in a heatmap (Figure 5D). Notably, two members of the solute carrier (SLC) protein encoding genes, *slc7a2* and *slc16a8*, were among the top 50 most significantly downregulated genes (black arrowheads in Figure 5D). Other genes of interest include the β -tubulin gene, *tubb5* (Baraban et al., 2013); a member of the biogenesis of lysosomal organelles complex 1 subunit 3, *bloc1s3* (Pennamen et al., 2021); and a member of the mitochondrial anion carrier protein, *ucp2* (Donadelli et al., 2014; pink arrowheads in Figure 5D). There were also a few DEGs that were mapped to uncharacterized genes, including *zgc:113278*, *zgc:92791*, and *zgc:86896*. The latter (i.e., *zgc:86896*) is predicted to participate in actin filament binding activity (ZFIN ID: ZDB-GENE-040625-80, 2022).

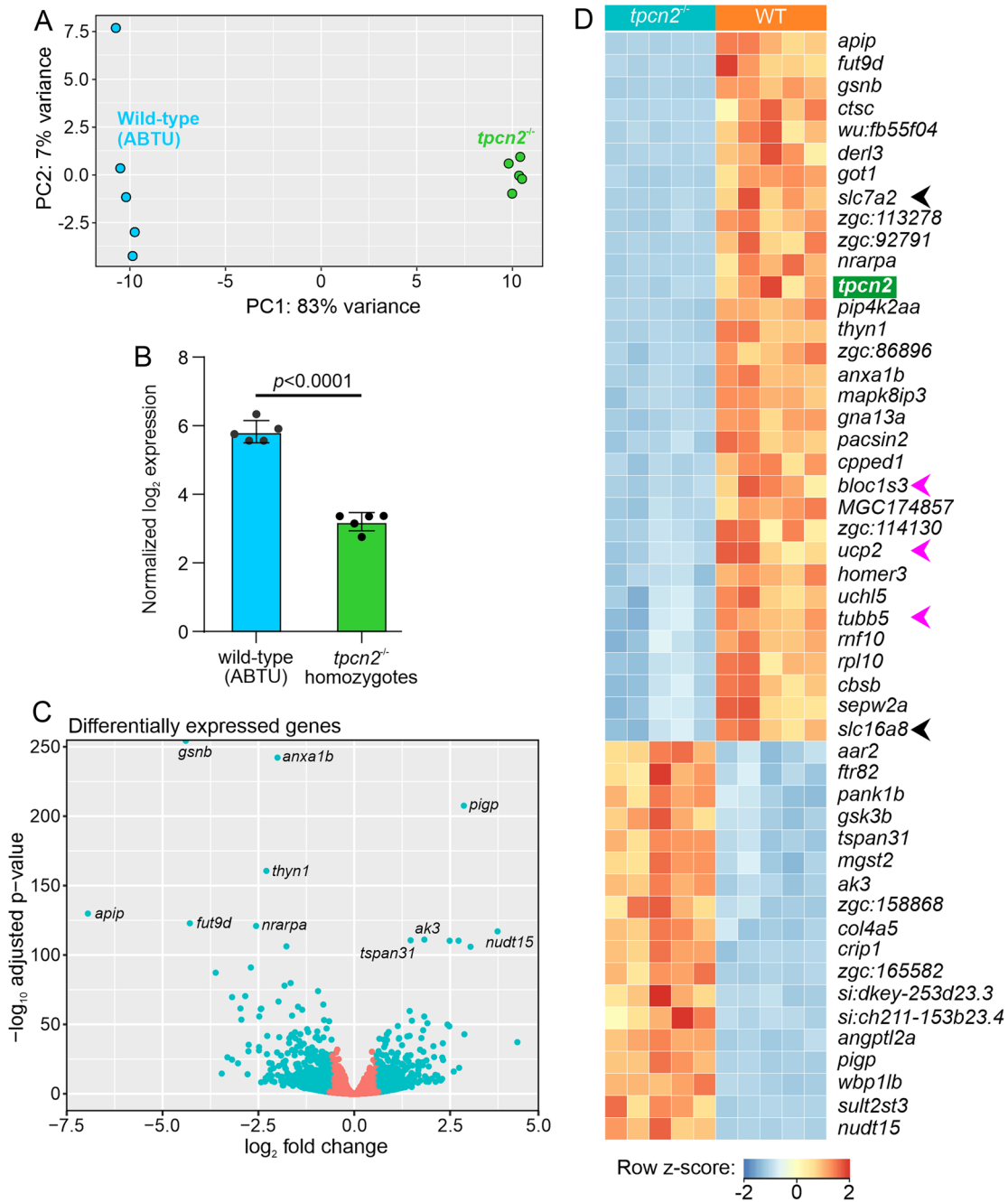


Figure 5. Principal components analysis (PCA) and differentially expressed genes (DEGs) in *tpcn2^{-/-}* mutants compared to wild-type (ABTU) controls. (A) PCA plot of the RNA-seq data from wild-type controls (blue; $n = 5$) and *tpcn2^{-/-}* mutants (green; $n = 5$). Each point represents one sample. (B) Normalized expression of *tpcn2* in the mutants compared to the wild-type embryos. The data were compared using one-way ANOVA followed by Tukey's test. (C) Volcano plot showing the DEGs. Those that passed the threshold for false discovery rate (FDR) and \log_2 fold change are indicated by a blue circle. The 10 most DEGs are labeled by their gene name. (D) Heatmap showing the top 50 significantly DEGs in the mutant embryos compared with ABTU wild-type embryos. The relative expression is indicated using a graded color-scale, where each gene is assigned a z-score depending on the respective amount of down- (shades of blue) or up- (shades of red) regulation between the samples. The gene names are shown on the right, and *tpcn2* is highlighted in green. The *slc* genes are indicated with black arrowheads, whereas *bloc1s3*, *ucp2*, and *tubb5* are indicated with pink arrowheads.

Disparate Biological Processes in *tpcn2*^{-/-} Mutants Compared to Wild-Type Controls

The significant DEGs were matched to the *D. rerio* genome in the Gene Ontology (GO) Consortium database to identify biological processes that were affected in the *tpcn2*^{-/-} mutants compared to the wild-type controls. The top 20 ranking GO terms that were enriched in the *tpcn2* mutants are summarized in Figure 6. Upregulated processes in the *tpcn2*^{-/-} mutants were mainly related to the response to extracellular signals (e.g., hormones; GO:0009725 and abiotic stimulus; GO:0009628), and biochemical processes involved in metabolism (e.g., the organic hydroxy compound metabolic process; GO:1901615 and organic acid metabolic process; GO:0006082). However, interestingly, the “negative regulation of secretion by cell” was also upregulated (GO:1903531), examples of which include *anxa1a* and *asip2b*. On the other hand, the downregulated processes in the *tpcn2*^{-/-} mutants included ECM binding (GO: 0050840; e.g., *lgals2b*), actin filament severing (GO: 0051014; e.g., *gsnb*), cellular component morphogenesis (GO:0032989; e.g., *notch1a*, *prdm14*, and *stmn4*), organelle assembly (GO: 0070925; e.g., *pacsin2*, *tspan4a*, and *dynlt5*), Ca²⁺ binding (GO:0005509; e.g., *actn2b*, *myl7*, and *syt11a*), and structural constituent of cytoskeleton (GO:0005200; e.g., *tuba2*, *tubb2*, and *viml*). Thus, our transcriptomic profiling data indicate that the *tpcn2*^{-/-} mutants have significantly attenuated gene expression patterns and disparate biological processes compared to the wild-type controls.

Discussion

Our *tpcn2* knockdown or knockout data revealed a distinct notochord phenotype. The gross morphology of embryos in which *tpcn2* was knocked down was normal except that body axis straightening was attenuated when compared with the controls (Figure 1). In addition, knockdown or knockout of *tpcn2* produced notochords with increased numbers of smaller, more spherical vacuoles when compared with the controls (Figures 2 and 3).

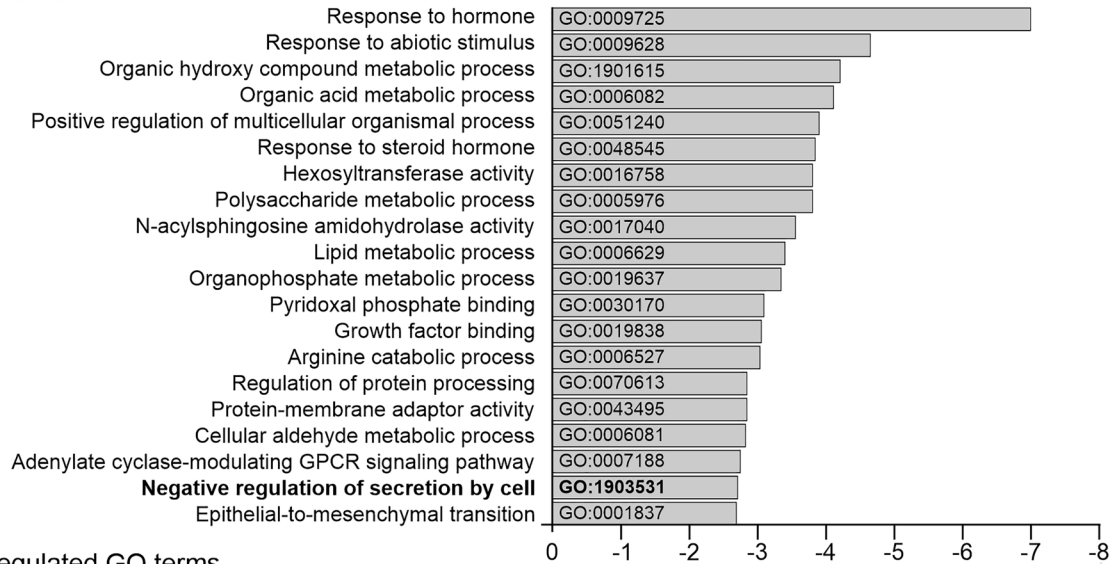
The spherical notochord vacuoles observed in the *tpcn2* mutants resemble the phenotype of other zebrafish mutants such as *snow white* and *mind bomb* (Stemple et al., 1996). Notably, the zebrafish *snow white* mutant has been proposed as a model for Hermansky-Pudlak Syndrome (HPS) Type 5, which is a genetic disease characterized by oculocutaneous hypopigmentation and bleeding diathesis (Daly et al., 2013). The *snow white* locus encodes HPS gene products belonging to subunits of the biogenesis of lysosome-related organelle complexes (Bloc) and the adaptor protein 3 complex (AP3) (Daly et al., 2013). These complexes are known to function in the trafficking of enzymes and precursor molecules to the melanosome (Huizing et al., 2008). Furthermore, the *snow white* mutant, which is deficient in *Hps5*, displays melanosome defects and hypopigmentation. Interestingly, the latter phenotype was also reported in

tpcn2 mutant zebrafish (Kelu et al., 2017), and pigmentation defects have also been reported in *Xenopus* oocytes with aberrant TPC2 expression (Lin-Moshier et al., 2014).

Our RNA-seq analysis identified *bloc1s3* as one of the top 50 most significantly downregulated genes in the *tpcn2* mutants (Figure 5D). This suggests that in these mutants, the biogenesis of lysosome-related organelles, which include notochord vacuoles, are affected (Setty et al., 2007). Unpublished work in Dr. Kathryn Ellis’ PhD thesis shows that *slc38a8b* morphants also have small and spherical notochord vacuoles (Ellis, 2014). Slc38a8b belongs to a family of Na⁺-dependent neutral amino acid transporters and at least one member of the SLC38 family has been shown to play a role in maintaining osmolyte balance and regulating the cell volume (Franchi-Gazzola et al., 2006). Thus, the small spherical notochord vacuole phenotype observed in the *slc38a8b* morphants was proposed to be a result of defects in amino acid transport into the vacuole, which would (under normal conditions), act to attract water into the vacuole lumen and result in osmotic-driven inflation (Ellis, 2014). Our RNA-seq data support these observations as among the DEGs in the *tpcn2*^{-/-} embryos, there were 37 members of the SLC family, with the expression of *slc7a2* being most significantly affected. Although *slc38a8b* was not identified among the DEGs, *slc38a11* and *slc38a2* were upregulated and downregulated, respectively in the mutants. It has previously shown that in MCF7 human breast cancer cells, SLC38A2 is localized to endosome-like vesicles and that knockdown of *SLC38A2* results in an inhibition of cell growth (Morotti et al., 2021). *tpcn2* mRNA is known to be expressed in MCF7 cells as well as various other tumorigenic and non-tumorigenic breast cell lines (Jahidin et al., 2016). Thus, our new data support the existing evidence for protein interactions between TPC2 and SLC family members (Krogsaeter et al., 2019). Therefore, we suggest that *slc7a2*, *slc38a11*, and *slc38a2* are candidates for further investigation into the possible roles of TPCs in amino acid transport and notochord vacuole inflation.

The evidence suggests that small, rounded notochord vacuoles are a hallmark of defects in lysosome-related organelle biogenesis and amino acid (and other solute) transport. However, while this might explain why the notochord vacuoles of *tpcn2* mutants do not appear to be fully inflated (given their small size relative to wild-type notochord vacuoles), it does not explain why the vacuoles are spherical in shape. The morphology of cells, as well as the shape and position of their intracellular organelles, is highly dependent on the arrangement and function of their cytoskeletal proteins (Brandizzi and Wasteneys, 2013), and the volume restriction imposed by the notochord sheath (Wopat et al., 2018). Actin filaments, intermediate filaments, and microtubules all function as scaffolds to transport and/or anchor organelles to their intracellular location (Pollard and Cooper, 2009; Stephens, 2012). For example, it has been shown that keratin (an

A Upregulated GO terms



B Downregulated GO terms

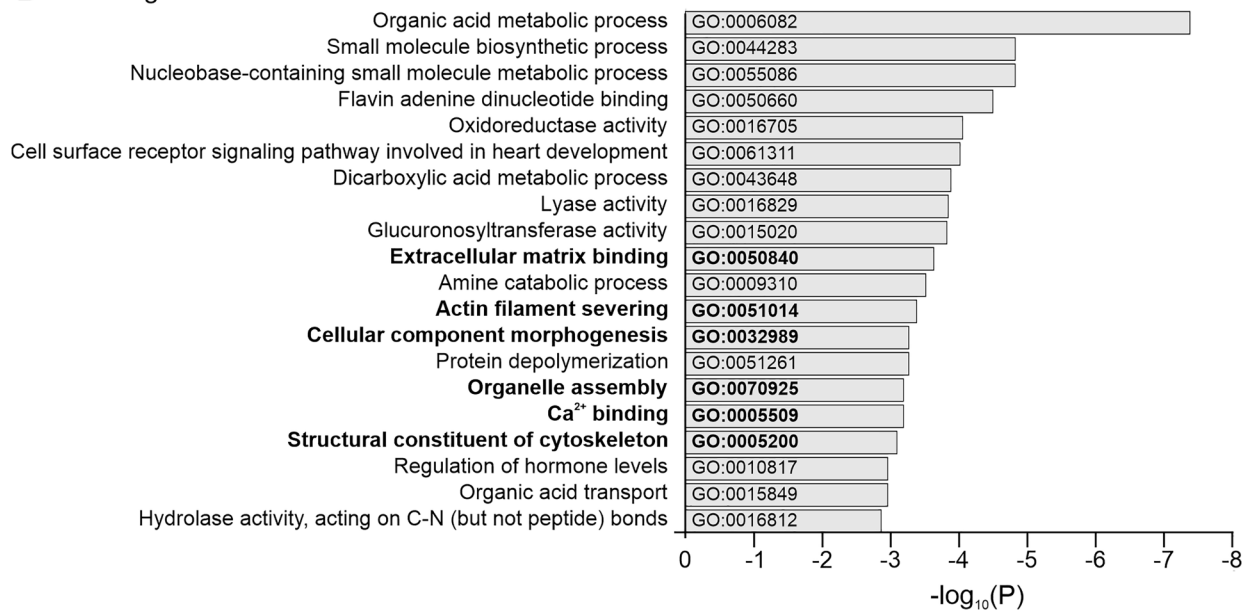


Figure 6. Top 20 gene ontology (GO) analysis terms that were enriched among the up- and downregulated genes in the *tpcn2*^{-/-} mutants compared to the wild-type controls. Horizontal bar graphs showing the (A) upregulated and (B) downregulated GO terms in the *tpcn2* homozygotes. The bar length represents the $-\log_{10} p$ value; the GO term ID is shown on the graph; and the full GO term is listed on the left.

intermediate filament protein) is enriched in the vacuolated notochord cells of the teleost, *Perca flavescens* (Schmitz, 1998). Using electron microscopy, Nixon et al. (2007) also identified keratin filaments associated with notochord caveolae in zebrafish embryos. These cell surface pits are especially densely packed in the central septa of the notochord, and they are suggested to buffer tension due to the mechanical stress exerted on these cells (Lim et al., 2017). While we did not investigate the localization of keratin in the notochord following *tpcn2* knockout, our RNA-seq data indicate that the keratin genes *krt1c19e* and *krt95* were both significantly

downregulated in these mutants, which might contribute to the phenotypic abnormalities observed.

It has been previously reported that keratin assembly relies on intact actin filaments and microtubules (Wöll et al., 2005; Kölsch et al., 2009). In this respect, our RNA-seq data show that *gsnb* is in the top 10 of the most significantly downregulated genes in the *tpcn2* mutants compared to the wild-type controls (Figure 5C and D). *gsnb* encodes a Ca²⁺-sensitive actin-depolymerizing factor, gelsolin, which plays an important role in modulating actin organization by severing and capping polymerizing actin filaments

(Sun et al., 1999). Likewise, our imaging data of ~24 hpf zebrafish embryos showed prominent F-actin labeling in the vacuolated notochord cells (Figure 4). This abundance of F-actin is in line with what has been reported previously in the zebrafish notochord (Daggett et al., 2007).

Given the Ca^{2+} -sensitivity of gelsolin (Gremm and Wegner, 2000), a role for TPC2-mediated Ca^{2+} signaling in shaping local or global Ca^{2+} transients required for cytoskeletal organization is a possibility. Our GO enrichment analysis of the *tpcn2* mutants supports this hypothesis, whereby “actin filament severing” (GO:0051014), “ Ca^{2+} binding” (GO:0005509), “organelle assembly” (GO:0070925), and “structural constituent of cytoskeleton” (GO:0005200) were among the top 20 downregulated GO terms (Figure 6).

Our images of embryos that were immunolabeled with the anti-TPC2 antibody lend further support to an emerging role for TPC2 in the developing notochord. Our data suggest that TPC2 is expressed in the notochord sheath and inner vacuolar cells, where it adopts a punctate appearance throughout the notochord (Figure 4). This is consistent with the expected pattern of a dynamic, lysosome-associated protein, rather than one that decorates the membrane of the notochord vacuole itself, such as Rab32a, which has been shown to label the vacuolar membrane (Ellis et al., 2013a). The pattern of TPC2-labeling displayed, closely resembles the punctate pattern of Lamp1 and Lamp2 in zebrafish notochords described previously (Ellis et al., 2013a). Our immunolabeling data also indicated distinct localization patterns of TPC2 in the nuclei of the notochord cells (Figure 4A). The nuclear localization of TPC2 has previously been described in differentiating slow muscle cells of zebrafish embryos (see Figure 5A and B in Kelu et al., 2015).

It has been suggested that there might be a possible evolutionary conservation of vacuolated cell biogenesis between animals and plants. The earliest studies that characterized TPCs were performed in *Arabidopsis thaliana*, which encodes one TPC isoform (AtTPC1) that is localized to the vacuolar membrane (i.e., the tonoplast). AtTPC1 was shown to generate slow vacuolar Ca^{2+} fluxes, which are involved in germination and stomatal opening (Furuichi et al., 2001; Peiter et al., 2005). Plant cell vacuoles are also known to play the equivalent of the lytic role of the lysosomes found in animal cells, and they are essential organelles for structural support, growth, protein storage, and response to the environment (Zhang et al., 2014). Like notochord vacuoles, the central vacuole in plant cells can occupy a significant volume of the cell (up to ~90%), and like lysosomes, the Ca^{2+} concentration inside plant vacuoles is significantly higher (i.e., up to ~1,000-fold) than the surrounding cytosol (Bush, 1993). While the protein machinery involved in vacuole fusion in plants is still under investigation, many components of this pathway, including the Rab-family GTPases, vacuolar SNAREs, and homotypic fusion and vacuole protein sorting complex proteins, as well as a requirement for localized Ca^{2+} transients in vacuole fusion

have been studied extensively in yeast (Burgoyne and Clague, 2003; Wickner, 2010; Parkinson et al., 2014). Several of these proteins, including Rab32a, Vps11, and Vps18, have also been implicated in zebrafish notochord vacuole biogenesis (Ellis et al., 2013a). Currently, knowledge on Ca^{2+} handling by notochord vacuolar cells in vertebrates is limited, although it has been suggested that Ca^{2+} channels such as members of the transient receptor potential (TRP) family of ion channels (e.g., TRPV4), might participate in osmoregulation and notochord vacuole volume (Ellis et al., 2013b).

Although we have not yet directly visualized Ca^{2+} signaling events during zebrafish vacuole biogenesis, we present indirect evidence that TPCs might be regulating a variety of required membrane contact events via the release of Ca^{2+} , as they have been reported to do in various other systems and cell types (Kinnear et al., 2004; Kilpatrick et al., 2017; Davis et al., 2020; Rice et al., 2022). Our data include treatment with the NAADP antagonist *trans*-Ned-19 (Figure 3), which was shown to have a significant effect on vacuole formation when compared with the DMSO solvent control, supporting the suggestion that TPC2 function was pharmacologically impaired. It was noted, however, that DMSO alone (at the concentration used) also had an effect on vacuole size compared to the untreated controls. This is perhaps not surprising as the effects of DMSO on the permeability of membranes are well recorded (Gironi et al., 2020).

The appearance of the notochord in *trans*-Ned-19 treated embryos (Figure 3) might be explained if the activity of TPC2 was regulated by the second messenger NAADP (Galione et al., 2022) during notochord biogenesis. This supports our suggestion that TPC2 might be mediating its effect partly via NAADP-triggered Ca^{2+} release during the development of the notochord vacuolated cells and associated sheath cells. With regards to the latter, Ca^{2+} signaling has also been reported to play a role in regulating the formation of the periderm, the embryonic sheath-like epithelium in gastrula stage zebrafish embryos (Zhang et al., 2011). We suggest that attenuation of TPC2-mediated Ca^{2+} release might contribute to the abnormalities in notochord formation observed and might underlie the attenuation in tail straightening. Furthermore, the fact that attenuated *tpcn2* expression also contributes to abnormal slow skeletal muscle phenotypes in zebrafish (Kelu et al., 2015, 2017) suggests that this might also contribute to the defects in trunk formation observed.

Vacuole biogenesis initially involves the formation of small pre-vacuoles followed by fusion events that eventually result in the formation of the larger main vacuole, with the entire process lasting ~4 h (Bagwell et al., 2020). Furthermore, if vacuole biogenesis is disrupted then this results in a deformed notochord containing many small vacuoles (Ellis, 2014). We propose that TPC2-mediated signaling might play a part in regulating the membrane contact

events involved in the formation and fusion of pre-vacuoles, and thus help regulate their fusion to the main cell vacuole. Such a role in vesicle fusion is consistent with what has been reported in other systems (Grimm et al., 2017). The smaller size of the notochord vacuoles in TPC2 morphants and mutants compared to the controls (Figure 3) suggests that pre-vacuole fusion to form the main vacuole is disrupted resulting in this notochord phenotype. A somewhat similar effect was observed when zebrafish embryos were treated with bafilomycin A1 to deplete the lysosomal acidic Ca^{2+} stores (Ellis, 2014).

In conclusion, we suggest that TPC2-mediated signaling might play a key role in regulating vesicle trafficking and fusion resulting from membrane contact events during notochord biogenesis in zebrafish embryos. Our new data support the proposition that vacuole inflation in the inner notochord cells provides a hydrostatic skeleton required for trunk straightening prior to bone osteogenesis.

Experimental Procedures

Zebrafish Husbandry

Wild-type AB and ABTU zebrafish were obtained from the Zebrafish International Resource Center (University of Oregon, Eugene, OR, USA), and Prof. Han Wang (Soochow University, Suzhou, China), respectively. Adult fish were maintained in Aquatic Habitat (AHAB) systems (Aquatic Eco-systems, Inc., Apopka, FL, USA) at $\sim 28^\circ\text{C}$ on a 14-h light/10-h dark cycle. Their fertilized eggs were obtained using well-established protocols (Westerfield, 2000), and then maintained in Danieau's solution (17.4 mM NaCl, 0.21 mM KCl, 0.12 mM $\text{MgSO}_4 \cdot 7\text{H}_2\text{O}$, 0.18 mM $\text{Ca}(\text{NO}_3)_2 \cdot 4\text{H}_2\text{O}$ and 1.5 mM HEPES; pH 7.2) until they reached ~ 17 hpf or ~ 24 hpf. All the procedures used in this study with zebrafish were conducted in accordance with the guidelines and regulations outlined by the Animal Ethics Committee of HKUST, and the Department of Health, Hong Kong.

MOs \pm mRNA Rescue, and Mutant Lines

All the MOs (Gene Tools LLC, Philomath, OS, USA) were prepared at a stock concentration of 1 mM in Milli-Q water and stored at room temperature. The expression of TPC2 was attenuated using a translation blocking *tpcn2*-MO (*tpcn2*-T-MO; described by Kelu et al., 2015). *p53*-MO (injected alone) and an SC-MO were also used as specificity controls (Kelu et al., 2015). The MOs were prepared and injected into AB wild-type embryos using methods described previously (Webb and Miller, 2013; Kelu et al., 2015).

The amounts of MOs injected are as follows:

- ~ 5 ng *p53*-MO or SC-MO (controls)
- ~ 2.5 ng *tpcn2*-T-MO + ~ 3.75 ng *p53*-MO (1:1.5 ratio)

In addition to using an MO to knock down *tpcn2* expression, we also used the *tpcn2*^{-/-} mutant line, which was generated as described previously (Kelu et al., 2017).

To visualize the effect of genetic knockdown or knockout of TPC2 on notochord vacuole inflation, bright-field images were acquired of wild-type AB embryos that had been injected with the MOs described above, and both wild-type (ABTU) and *tpcn2*^{-/-} mutant embryos, at ~ 24 hpf. To quantify the shape of the notochord vacuoles, the perimeter of each vacuole was traced, and a "circularity" value was obtained using the "Analyze > Measure" function in ImageJ (National Institutes of Health, Bethesda, MD, USA; <https://imagej.nih.gov/ij/>). Ten vacuoles per embryo were measured. A circularity value of 1 signifies a perfect circle, whereas a value closer to 0 indicates an elongated polygon. In addition, the number of vacuoles was quantified within an ROI of $80\ \mu\text{m} \times 250\ \mu\text{m}$. This is approximately equivalent to the width of 3 somites in wild-type/control embryos at ~ 24 hpf.

In some experiments, morphant and mutant embryos at $\sim 75\%$ epiboly (~ 8 hpf) were incubated overnight in Danieau's containing $25\ \mu\text{M}$ BODIPY® FL C₅-ceramide (ThermoFisher Scientific, Inc., MA, USA). They were then washed with Danieau's solution and anaesthetized in Danieau's solution containing 0.02% MS-222 (Sigma-Aldrich Corp., Merck Group, MI, USA) prior to imaging via confocal microscopy at ~ 24 hpf. The inner notochord cell area was quantified with the "Analyze > Measure" function in ImageJ. Again, ten vacuoles per embryo were measured.

Pharmacological Treatment of Embryos

A stock solution of 50 mM *trans*-Ned-19 (Enzo Life Sciences, NY, USA) was prepared in DMSO and stored at -20°C . Just prior to use, stock *trans*-Ned-19 was diluted in Danieau's solution to $100\ \mu\text{M}$ and heated to 65°C for 5 min to prevent precipitation. It was then cooled to $\sim 28^\circ\text{C}$ before incubating with embryos. To visualize the effect of *trans*-Ned-19 on notochord vacuole inflation, embryos were first bathed in Danieau's containing $25\ \mu\text{M}$ BODIPY® FL C₅-ceramide from $\sim 75\%$ epiboly (~ 8 hpf) until the 15-somite stage (~ 17 hpf) to label the notochord cell membranes. The embryos were then bathed in Danieau's solution containing $100\ \mu\text{M}$ *trans*-Ned-19 (in a final DMSO concentration of $\sim 0.2\%$) or 0.25% DMSO alone (control) at $\sim 28^\circ\text{C}$ for 7 h, after which they were washed twice with Danieau's solution and anaesthetized with 0.02% MS-222 prior to imaging at ~ 24 hpf.

Whole-Mount Immunohistochemistry to Visualize TPC2

Embryos at ~ 24 hpf were dechorionated and fixed with phosphate-buffered saline (PBS; 137 mM NaCl, 2.68 mM

KCl, 16 mM Na₂HPO₄, 4 mM NaH₂PO₄·2H₂O, pH7.3) containing 4% paraformaldehyde overnight at 4 °C. After fixation, excess paraformaldehyde was removed and the embryos were washed first with PBS and then with PBS containing 0.2% Triton X-100 (PBST), after which they were permeabilized with PBST containing 1% DMSO (PBSTD) for 1 h. Permeabilized embryos were then incubated with blocking buffer (PBST containing 10% goat serum and 1% bovine serum albumin; Sigma-Aldrich Corp.) for 2 h, after which they were incubated with blocking buffer containing the anti-TPCN2 (code # A17271, ABclonal Science Inc., MA, USA) primary antibody (used at 1:25 dilution) at ~4 °C for 2 days. After the primary antibody incubation step, embryos were then washed extensively before being incubated with an Alexa Fluor 488 F(ab')₂ goat anti-rabbit IgG (H+L) antibody (used at 1:200; code # A11070; ThermoFisher Scientific, Inc.) at ~4 °C overnight in the dark. The embryos were then incubated with Alexa Fluor 568-phalloidin (used at 1:50; code # A12380, ThermoFisher Scientific, Inc.) and 1 µg/mL Hoechst 33258 (Code # H-21491, ThermoFisher Scientific, Inc.) at room temperature for 1 h in the dark to label F-actin and the nuclei, respectively. The embryos were washed extensively with wash buffer (i.e., blocking buffer at 1:10 dilution) between each incubation step. At the end of the final wash steps, the labeled embryos were washed with PBST and then with PBS. To improve the incubation and washing efficiencies, gentle shaking was applied throughout using a mini gyro-rocker (Techne SSM3, Cole-Parmer, Stone, UK). Working dilutions of the antibodies and phalloidin were prepared in blocking buffer followed by centrifugation at 16,873×g for 5 min to pellet any unwanted debris. Although no specificity control was run by labeling morphants or mutants with the anti-TPCN2 antibody, the antibody was previously used to immunolabel the neuromasts and olfactory organs of zebrafish larvae (Choi et al., 2022).

Bright-Field and Confocal Imaging

Fixed and live embryos were imaged using a Leica TCS SP8 laser scanning confocal microscope (Leica Microsystems GmbH, Wetzlar, Germany) with HC PL APO 40x/1.30 and HC PL APO 60x/1.40 oil objective lenses. Live embryos were anaesthetized for ~5 min before the start of imaging by immersion in Danieau's solution containing ~0.02% MS-222. For all embryos, the notochord located in the anterior region of the trunk adjacent to somites 7–11 (unless otherwise stated), was imaged from a lateral view, anterior to the left. The respective wavelengths (excitation/detection) of the various fluorophores used, are as follows: Alexa Fluor 488 and BODIPY FL C₅ ceramide (488 nm/519 nm); Alexa Fluor 568 (568 nm/600 nm); and Hoechst 33258 (350 nm/461 nm). The temperature was maintained at ~28 °C for all live imaging experiments using a heated imaging chamber (TOKAI HIT Stage Top Incubator®, Shizuoka-ken, Japan).

Preparation of Samples for RNA-Sequencing (RNA-seq)

Embryos were collected from wild-type (ABTU) and *tpcn2*^{-/-} mutants (Kelu et al., 2017), and maintained in Danieau's solution at ~28 °C. At ~17 hpf, the embryos were dechorionated via incubation in Danieau's solution containing 2 mg/mL pronase (Sigma-Aldrich Corp.) and gentle pipetting using a fire-polished Pasteur pipette. The dechorionated embryos were then transferred into fresh Danieau's solution. A pool of 80 ABTU or 80 *tpcn2*^{-/-} embryos (with five biological replicates for each group) were then transferred into a 1.5 mL centrifuge tube containing 500 µL RNazol® (Molecular Research Center, Inc., OH, USA) and immediately homogenized by trituration through a P200 pipette tip. The homogenate was then vigorously vortexed for 1 min to ensure complete cell lysis. Subsequently, RNA extraction was performed using RNazol® according to the manufacturer's instructions. The extracted RNA was then resuspended in 30 µL RNase-free water and kept at -80 °C. The concentration and quality of RNA were evaluated with a NanoDrop 2000 spectrophotometer (ThermoFisher Scientific, Inc.), and the integrity of the RNA was verified using an HS RNA kit (Agilent Technologies, CA, USA) and a 5200 Fragment Analyzer system (Agilent Technologies). RNA samples with purity (260/280 ratio) > 1.8 and RNA quality number (RQN) > 8.0 were submitted to the Biosciences Central Research Facility (BioCRF, HKUST) for RNA-sequencing (RNA-seq) with a BGI DNBSEQ-G400 sequencer (Beijing Genomics Institute, SC, China).

Bioinformatic Analysis of RNA-seq

The HKUST BioCRF processed the RNA-seq data as follows: adapter trimming, RSeQC analysis; read alignment to the GRCz11.94 (danRer11) zebrafish reference genome using STAR; and differential gene expression analysis using DESeq2. Pairwise comparisons were performed using the DESeq2 package (Love et al., 2014). A list of DEGs was obtained using cut-off values of Benjamini-Hochberg adjusted $p < .05$ and |Fold change| > 1.5. The data were then imported into R Studio (Version 2021.09.1 + 372; <https://www.rstudio.com/>; Boston, MA, USA), and the normalized counts of these genes were used to plot heatmaps with hierarchical clustering, via the pheatmap package. Gene ontology (GO)-term enrichment analysis was performed with Metascape (<https://metascape.org/gp/index.html#/main/step1>; Zhou et al., 2019).

Statistical Analysis and Figure Preparation

All image measurements were conducted with ImageJ. Numerical data were exported to Microsoft Office Professional Plus Excel 2013 (Microsoft Corp., WA, USA) for basic descriptive statistics and to GraphPad Prism (GraphPad Software, San Diego, CA, USA) for graph

plotting. Data were imported into Minitab 17.3.1 to conduct one-way ANOVA followed by Fisher's least significant difference or Tukey's test. Figures were prepared using CorelDRAW version 24 (Corel Corp., Ottawa, ON, Canada).

Acknowledgements

We thank Prof. John Parrington (University of Oxford, UK) for designing and providing us with the *tpcn*-MOs.

Data Availability

The RNAseq data can be found in NCBI's Gene Expression Omnibus and are accessible through GEO Series accession number GSE229162 (<https://www.ncbi.nlm.nih.gov/geo/query/acc.cgi?acc=GSE229162>).

Declaration of Conflicting Interests

The authors declared no potential conflicts of interest with respect to the research, authorship, and/or publication of this article.


Funding

The authors disclosed receipt of the following financial support for the research, authorship, and/or publication of this article: The Hong Kong Research Grants Council General Research Fund (grant number 16100719) and The Hong Kong Innovation and Technology Commission (grant number ITCPD/17-9).

Ethics Statement

All zebrafish experiments were conducted in accordance with the guidelines and regulations outlined by the Animal Ethics Committee of HKUST, and the Department of Health, Hong Kong.

ORCID iD

Sarah E. Webb  <https://orcid.org/0000-0002-0108-6606>

References

The authors in bold contributed equally as first authors. Ambrosio AL, Boyle JA, Aradi AE, Christian KA, Santiago M, Di Petro M (2016). TPC2 Controls pigmentation by regulating melanosome pH and size. *Proc Natl Acad Sci USA* 113, 5622–5627. doi: 10.1073/pnas.1600108113

Bagnat M, Gray RS (2020). Development of a straight vertebrate body axis. *Development* 147(21), dev175794. doi: 10.1242/dev.175794

Bagwell J, Norman J, Ellis K, Peskin B, Hwang J, Ge X, Nguyen SV, McMenamin SK, Stainier DY, Bagnat M (2020). Notochord vacuoles absorb compressive bone growth during zebrafish spine formation. *ELife* 9, e51221. doi: 10.7554/eLife.51221

Baraban M, Anselme I, Schneider-Maunoury S, Giudicelli F (2013). Zebrafish embryonic neurons transport messenger RNA to axons and growth cones *in vivo*. *J Neurosci* 33(4), 15726–15734. doi: 10.1523/JNEUROSCI.1510-13.2013

Barresi MJ, Stickney HL, Devoto SH (2000). The zebrafish *slow-muscle-omitted* gene product is required for Hedgehog signal transduction and the development of slow muscle identity. *Development* 127(10), 2189–2199. doi: 10.1242/dev.127.10.2189

Brandizzi F, Wasteneys GO (2013). Cytoskeleton-dependent endomembrane organization in plant cells: An emerging role for microtubules. *Plant J* 75(2), 339–349. doi: 10.1111/tpj.12227

Burgoyne RD, Clague MJ (2003). Calcium and calmodulin in membrane fusion. *Biochim Biophys Acta Mol Cell Res* 1641(2), 137–143. doi: 10.1016/S0167-4889(03)00089-2

Bush DS (1993). Regulation of cytosolic calcium in plants. *Plant Physiol* 103(1), 7–13. doi: 10.1104/pp.103.1.7

Cang C, Zhou Y, Navarro B, Seo Y, Aranda K, Shi L, Battaglia-Hsu S, Nissim I, Clapham DE, Ren D (2013). Mtor regulates lysosomal ATP-sensitive two-pore Na⁺ channel to adapt to metabolic state. *Cell* 152(4), 778–790. doi: 10.1016/j.cell.2013.01.023

Capel RA, Bolton EL, Lin WK, Aston D, Wang Y, Liu W, Wang X, Burton R-AB, Bloor-Young D, Shade K-T, et al. (2015). Two-pore channels (TPC2 s) and nicotinic acid adenine dinucleotide phosphate (NAADP) at lysosomal-sarcoplasmic reticular junctions contribute to acute and chronic β -adrenoceptor signaling in the heart. *J Biol Chem* 290(50), 30087–30098. doi: 10.1074/jbc.M115.684076

Chazotte B (2008). Labeling the Golgi apparatus with BODIPY-FL-Ceramide (C5-DMB-ceramide) for imaging. *CSH Protoc*. doi: 10.1101/pdb.prot4931

Choi SSA, Chan HH, Chan CM, Wang X, Webb SE, Leung KW, Tsim KW, Miller AL (2022). Neuromasts and olfactory organs of zebrafish larvae represent possible sites of SARS-Cov-2 pseudovirus host cell entry. *J Virol* 96, 24. doi: 10.1128/jvi.01418-22

Cleaver O, Seufert DW, Krieg PA (2000). Endoderm patterning by the notochord: Development of the hypochord in *Xenopus*. *Development* 127(4), 869–879. doi: 10.1242/dev.127.4.869

Corralo D, Trapani V, Bonaldo P (2015). The notochord: Structure and functions. *Cell Mol Life Sci* 72(16), 2989–3008. doi: 10.1007/s00018-015-1897-z

Coutinho P, Parsons MJ, Thomas KA, Hirst EMA, Saúde L, Campos I, Williams PH, Stemple DL (2004). Differential requirements for COPI transport during vertebrate early development. *Dev Cell* 7, 547–558. doi: 10.1016/j.devcel.2004.07.020

Daggett DF, Domingo CR, Currie PD, Amacher SL (2007). Control of morphogenetic cell movements in the early zebrafish myotome. *Dev Biol* 309(2), 169–179. doi: 10.1016/j.ydbio.2007.06.008

Daly CMS, Willer J, Gregg R, Gross JM (2013). *Snow white*, a zebrafish model of Hermansky-Pudlak syndrome type 5. *Genetics* 195(2), 481–494. doi: 10.1534/genetics.113.154898

Davidson SM, Foote K, Kunuthur S, Gosain R, Tan N, Tyser R, Zhao YJ, Graeff R, Ganesan A, Duchon MR, et al. (2015). Inhibition of NAADP signalling on reperfusion protects the heart by preventing lethal calcium oscillations via two-pore channel 1 and opening of the mitochondrial permeability transition pore. *Cardiovasc Res* 108(3), 357–366. doi: 10.1093/cvr/cvv226

Davis LC, Morgan AJ, Chen J-L, Snead CM, Bloor-Young D, Shenderov E, Stanton-Humphreys MN, Conway SJ, Churchill GC, Parrington J, et al. (2012). NAADP Activates two-pore channels on T cell cytolytic granules to stimulate exocytosis and killing. *Curr Biol* 22, 2331–2337. doi: 10.1016/j.cub.2012.10.035

Davis LC, Morgan AJ, Galione A (2020). NAADP-regulated two-pore channels drive phagocytosis through endo-lysosomal Ca²⁺ nanodomains, calcineurin and dynamin. *EMBO J* 39(14), e104058. doi: 10.15252/embj.2019104058

Donadelli M, Dando I, Fiorini C, Palmieri M (2014). UCP2, A mitochondrial protein regulated at multiple levels. *Cell Mol Life Sci* 71, 1171–1190. doi: 10.1007/s00018-013-1407-0

- Dong X-P, Shen D, Wang X, Dawson T, Li X, Zhang Q, Cheng X, Zhang Y, Weisman LS, Dellling M, Xy H (2010). PI(3,5)P₂ controls membrane trafficking by direct activation of mucolipin Ca²⁺ release channels in the endosome. *Nature Comm* 1, 38. doi: 10.1038/ncomms1037
- Edgar R, Domrachev M, Lash AE (2002). Gene expression omnibus: NCBI gene expression and hybridization array data repository. *Nucleic Acids Res* 30(1), 207–210.
- Ellis K, Bagwell J, Bagnat M (2013a). Notochord vacuoles are lysosome-related organelles that function in axis and spine morphogenesis. *J Cell Biol* 200(5), 667–679. doi: 10.1083/jcb.201212095
- Ellis K, Hoffman BD, Bagnat M (2013b). The vacuole within: How cellular organization dictates notochord function. *BioArch* 3(3), 64–68. doi: 10.4161/bioa.25503
- Ellis KL (2014). *Molecular Mechanisms of Notochord Vacuole Formation and Their Role in Zebrafish Development*. <https://dukespace.lib.duke.edu/dspace/handle/10161/8723>
- Franchi-Gazzola R, Dall'Asta V, Sala R, Visigalli R, Bevilacqua E, Gaccioli F, Gazzola GC, Bussolati O (2006). The role of the neutral amino acid transporter SNAT2 in cell volume regulation. *Acta Physiol* 187(1–2), 273–283. doi: 10.1111/j.1748-1716.2006.01552.x
- Furuichi T, Cunningham KW, Muto S (2001). A putative two pore channel AtTPC1 mediates Ca²⁺ flux in *Arabidopsis* leaf cells. *Plant Cell Physiol* 42(9), 900–905. doi: 10.1093/pcp/pce145
- Galione A, Davis LC, Martucci L, Morgan AJ (2022). NAADP-Mediated Ca²⁺ Signalling. Berlin, Heidelberg: Handb Exp Pharmacol, Springer. doi: 10.1007/164_2022_607
- García-Rúa V, Feijóo-Bandín S, Rodríguez-Penas D, Mosquera-Leal A, Abu-Assi E, Beiras A, Seoane LM, Lear P, Parrington J, Portolés M, et al. (2016). Endolysosomal two-pore channels regulate autophagy in cardiomyocytes. *J Physiol* 594(11), 3061–3077. doi: 10.1113/JP271332
- Gironi B, Kahveci Z, McGill B, Lechner B-D, Pagliari S, Metz J, Morresi A, Palombo F, Sassi P, Petrov PG (2020). Effect of DMSO on the mechanical and structural properties of model and biological membranes. *Biophys J* 119, 274–286. doi: 10.1016/j.bpj.2020.05.037
- Glickman NS, Kimmel CB, Jones MA, Adams RJ (2003). Shaping the zebrafish notochord. *Development* 130(5), 873–887. doi: 10.1242/dev.00314
- Gremm D, Wegner A (2000). Gelsolin as a calcium-regulated actin filament-capping protein. *Eur J Biochem* 267(14), 4339–4345. doi: 10.1046/j.1432-1327.2000.01463.x
- Grimm C, Chen C-C, Wahl-Schott C, Biel M (2017). Two-pore channels: Catalyzers of endolysosomal transport and function. *Front Pharmacol* 8, 45. doi: 10.3389/fphar.2017.00045
- Gunaratne GS, Yang Y, Li F, Walseth TF, Marchant JS (2018). NAADP-dependent Ca²⁺ signaling regulates Middle East respiratory syndrome-coronavirus pseudovirus translocation through the endolysosomal system. *Cell Calcium* 75, 30–41. doi: 10.1016/j.ceca.2018.08.003
- Guo C, Webb SE, Chan CM, Miller AL (2020). TPC2-mediated Ca²⁺ signaling is required for axon extension in caudal primary motor neurons in zebrafish embryos. *J Cell Sci* 133(13), jcs244780. doi:10.1242/jcs.244780
- Hejnal A, Lowe CJ (2014). Animal evolution: Stiff or squishy notochord origins? *Curr Biol* 24(23), R1131–R1133. doi: 10.1016/j.cub.2014.10.059
- Hu M, Zhou N, Cai W, Xu H (2022). Lysosomal solute and water transport. *J Cell Biol* 227(11), e202109133. doi: 10.1083/jcb.202109133
- Huizing M, Helip-Wooley A, Westbroek W, Gunay-Aygun M, Gahl WA (2008). Disorders of lysosome-related organelle biogenesis: Clinical and molecular genetics. *Annu Rev Genomics Hum Genet* 9, 359–386. doi: 10.1146/annurev.genom.9.081307.164303
- Hunter CJ, Bianchi S, Cheng P, Muldrew K (2007). Osmoregulatory function of large vacuoles found in notochordal cells of the intervertebral disc. *Mol Cell Biomech* 4(4), 227–237.
- Jahidin AH, Stewart TA, Thompson EW, Roberts-Thomson SJ, Monteith GR (2016). Differential effects of two-pore channel protein 1 and 2 silencing in MDA-MB-468 breast cancer cells. *Biochem Biophys Res Commun* 477, 731–736. doi: 10.1016/j.bbrc.2016.06.127
- Jin X, Zhang Y, Alharbi A, Hanbashi A, Alhoshani A, Parrington J (2020). Targeting two-pore channels: Current progress and future challenges. *Trends Pharmacol Sci* 41(8), 582–594. doi: 10.1016/j.tips.2020.06.002
- Kelu JJ, Chan HLH, Webb SE, Cheng AHH, Ruas M, Parrington J, Galione A, Miller AL (2015). Two-pore channel 2 activity is required for slow muscle cell-generated Ca²⁺ signaling during myogenesis in intact zebrafish. *Int J Dev Biol* 59(7–8–9), 313–325. doi: 10.1387/ijdb.150206am
- Kelu JJ, Webb SE, Parrington J, Galione A, Miller AL (2017). Ca²⁺ release via two-pore channel type 2 (TPC2) is required for slow muscle cell myofibrillogenesis and myotomal patterning in intact zebrafish embryos. *Dev Biol* 425(2), 109–129. doi: 10.1016/j.ydbio.2017.03.031
- Kilpatrick BS, Eden ER, Hockey LN, Yates E, Futter CE, Patel S (2017). An endosomal NAADP-sensitive two-pore Ca²⁺ channel regulates ER-endosome membrane contact sites to control growth factor signaling. *Cell Rep* 18(7), 1636–1645. doi: 10.1016/j.celrep.2017.01.052
- Kilpatrick BS, Eden ER, Schapira AH, Futter CE, Patel S (2013). Direct mobilization of lysosomal Ca²⁺ triggers complex Ca²⁺ signals. *J Cell Sci* 126, 60–66. doi:10.1242/jcs.118836
- Kinnear NP, Boittin F-X, Thomas JM, Galione A, Evans AM (2004). Lysosome-sarcoplasmic reticulum junctions. A trigger zone for calcium signaling by nicotinic acid adenine dinucleotide phosphate and endothelin-1. *J Biol Chem* 279(52), 54319–54326. doi: 10.1074/jbc.M406132200
- Kinoshita T, Fujita M (2016). Biosynthesis of GPI-anchored proteins: Special emphasis on GPI lipid remodeling. *J Lipid Res* 57(1), 6–24. doi: 10.1194/jlr.R063313
- Kölsch A, Windoffer R, Leube RE (2009). Actin-dependent dynamics of keratin filament precursors. *Cell Motil Cytoskel* 66(11), 976–985. doi: 10.1002/cm.20395
- Krogsaeter EK, Biel M, Wahl-Schott C, Grimm C (2019). The protein interaction networks of mucolipins and two-pore channels. *Biochim Biophys Acta Mol Cell Res* 1866(7), 1111–1123. doi: 10.1016/j.bbamcr.2018.10.020
- Li S, Cerri M, Strazzer P, Li Y, Spelt C, Blied M, Vandenbussche M, Martínez-Calvo E, Lai B, Reale L, Koes R, Quattrocchio FM (2021). An ancient RAB5 governs the formation of additional vacuoles and cell shape in petunia petals. *Cell Rep* 36(13), 109749. doi: 10.1016/j.celrep.2021.109749
- Lim Y-W, Lo HP, Ferguson C, Martel N, Giacomotto J, Gomez GA, Yap AS, Hall TE, Parton RG (2017). Caveolae protect notochord cells against catastrophic mechanical failure during development. *Curr Biol* 27(13), 1968–1981.e7. doi: 10.1016/j.cub.2017.05.067
- Lin P-H, Duann P, Komazaki S, Park KH, Li H, Sun M, Sermersheim M, Gumpfer K, Parrington J, Galione A, et al. (2015). Lysosomal two-pore channel subtype 2 (TPC2) regulates

- skeletal muscle autophagic signaling. *J Biol Chem* 290(6), 3377–3389. doi: 10.1074/jbc.M114.608471
- Lin-Moshier Y, Keebler MV, Hooper R, Boulware MJ, Liu X, Churamani D, Abood ME, Walseth TF, Brailoiu E, Patel S, Marchant JS (2014). The two-pore channel (TPC) interactome unmasks isoform-specific roles for TPCs in endolysosomal morphology and cell pigmentation. *Proc Natl Acad Sci USA* 111(36), 13087–13092. doi: 10.1073/pnas.1407004111
- Love MI, Huber W, Anders S (2014). Moderated estimation of fold change and dispersion for RNA-seq data with DESeq2. *Genome Biol* 15, 550. doi: 10.1186/s13059-014-0550-8
- Marchant JS, Patel S (2015). Two-pore channels at the intersection of endolysosomal membrane traffic. *Biochem Soc Trans* 43(3), 434–441. doi: 10.1042/BST20140303
- Mary C, Duek P, Salleron L, Tienz P, Bumann D, Bairoch A, Lane L (2012). Functional identification of APIP as human mtnB, a key enzyme in the methionine salvage pathway. *PLoS ONE* 7(12), e52877. doi: 10.1371/journal.pone.0052877
- McCann MR, Séguin CA (2016). Notochord cells in intervertebral disc development and degeneration. *J Dev Biol* 4(1), 3. doi: 10.3390/jdb4010003
- McCann MR, Tamplin OJ, Rossant J, Séguin CA (2012). Tracing notochord-derived cells using a *Noto-cre* mouse: Implications for intervertebral disc development. *Dis Model Mech* 5(1), 73–82. doi: 10.1242/dmm.008128
- Miyaji H, Yoshimoto T, Asakura H, Komachi A, Kamiya S, Takasaki M, Mizuguchi J (2002). Molecular cloning and characterization of the mouse thymocyte protein gene. *Gene* 297, 189–196. doi: 10.1016/S0378-1119(02)00886-7
- Morotti M, Zois CE, El-Ansari R, Craze ML, Rakha EA, Fan S-J, Valli A, Haider S, Goberdhan DCI, Green AR, Harris AL (2021). Increased expression of glutamine transporter SNAT2/SLC38A2 promotes glutamine dependence and oxidative stress resistance, and is associated with worse prognosis in triple-negative breast cancer. *Br J Cancer* 124, 494–505. doi: 10.1038/s41416-020-01113-y
- Nixon SJ, Carter A, Wegner J, Ferguson C, Floetenmeyer M, Riches J, Key B, Westerfield M, Parton RG (2007). Caveolin-1 is required for lateral line neuromast and notochord development. *J Cell Sci* 120(13), 2151–2161. doi: 10.1242/jcs.003830
- Parkinson K, Baines AE, Keller T, Gruenheit N, Bragg L, North RA, Thompson CRL (2014). Calcium-dependent regulation of Rab activation and vesicle fusion by an intracellular P2X ion channel. *Nat Cell Biol* 16(1), 87–98. doi: 10.1038/ncb2887
- Peiter E, Maathuis FJM, Mills LN, Knight H, Pelloux J, Hetherington AM, Sanders D (2005). The vacuolar Ca²⁺-activated channel TPC1 regulates germination and stomatal movement. *Nature* 434(7031), 404–408. doi: 10.1038/nature03381
- Pennamen P, Tingaud-Sequeira A, Michaud V, Morice-Picard F, Plaisant C, Vincent-Delorme C, Giuliano F, Azarnoush S, Capri Y, Marçon C, et al. (2021). Novel variants in the *BLOC1S3* gene in patients presenting a mild form of Hermansky-Pudlak syndrome. *Pigment Cell Melanoma Res* 34(1), 132–135. doi: 10.1111/pcmr.12915
- Pitt SJ, Funnell TM, Sitsapesan M, Venturi E, Rietdorf K, Ruas M, Ganesan A, Gosain R, Churchill GC, Zhu MX, et al. (2010). TPC2 Is a novel NAADP-sensitive Ca²⁺ release channel operating as a dual sensor of luminal pH and Ca²⁺. *J Biol Chem* 285(45), 35039–35046. doi: 10.1074/jbc.M110.156927
- Pollard TD, Cooper JA (2009). Actin, a central player in cell shape and movement. *Science* 326(5957), 1208–1212. doi: 10.1126/science.1175862
- Raynal P, Pollard HB (1994). Annexins: The problem of assessing the biological role for a gene family of multifunctional calcium- and phospholipid-binding proteins. *Biochem Biophys Acta* 1197(1), 63–93. doi: 10.1016/0304-4157(94)90019-1
- Rice KL, Webb SE, Miller AL (2022). Localized TPC1-mediated Ca²⁺ release from endolysosomes contributes to myoseptal junction development in zebrafish. *J Cell Sci* 135, jcs259564. doi: 10.1242/jcs.259564
- Robu ME, Larson JD, Nasevicius A, Beiraghi S, Brenner C, Farber SA, Ekker SC (2007). P53 activation by knockdown technologies. *PLoS Gen* 3(5), e78. doi: 10.1371/journal.pgen.0030078
- Ruas M, Chuang KT, Davis LC, Al-Douri A, Tynan PW, Tunn R, Teboul L, Galione A, Parrington J (2014). TPC1 Has two variant isoforms, and their removal has different effects on endolysosomal functions compared to loss of TPC2. *Mol Cell Biol* 34(21), 3981–3992. doi: 10.1128/MCB.00113-14
- Ruas M, Rietdorf K, Arredouani A, Davis LC, Lloyd-Evans E, Koegel H, Funnell TM, Morgan AJ, Ward JA, Watanabe K, et al. (2010). Purified TPC isoforms form NAADP receptors with distinct roles for Ca²⁺ signaling and endolysosomal trafficking. *Curr Biol* 20(8), 703–709. doi: 10.1016/j.cub.2010.02.049
- Sakurai Y, Kolokoltsov AA, Chen CC, Tidwell MW, Bauta WE, Klugbauer N, Grimm C, Wahl-Schott C, Biel M, Davey RA (2015). Two-pore channels control Ebolavirus host cell entry and are drug targets for disease treatment. *Science* 347(6225), 995–998. doi: 10.1126/science.1258758
- Schmitz RJ (1998). Immunohistochemical identification of the cytoskeletal elements in the notochord cells of bony fishes. *J Morphol* 236(2), 105–116. doi: 10.1002/(SICI)1097-4687(199805)236:2<105::AID-JMOR2>3.0.CO;2-4
- Setty SRG, Tenza D, Truschel ST, Chou E, Sviderskaya EV, Theos AC, Lamoreux ML, Di Pietro SM, Starcevic M, Bennett DC, et al. (2007). BLOC-1 is required for cargo-specific sorting from vacuolar early endosomes toward lysosome-related organelles. *Mol Biol Cell* 18, 768–780. doi: 10.1091/mbc.E06-12-1066
- Stemple DL (2005). Structure and function of the notochord: An essential organ for chordate development. *Development* 132(11), 2503–2512. doi: 10.1242/dev.01812
- Stemple DL, Solnica-Krezel L, Zwartkruis F, Neuhauss SC, Schier AF, Malicki J, Stainier DY, Abdelilah S, Rangini Z, Mountcastle-Shah E, Driever W (1996). Mutations affecting development of the notochord in zebrafish. *Development* 123(1), 117–128. doi: 10.1242/dev.123.1.117
- Stephens DJ (2012). Functional coupling of microtubules to membranes – implications for membrane structure and dynamics. *J Cell Sci* 125(12), 2795–2804. doi: 10.1242/jcs.097675
- Sun HQ, Yamamoto M, Mejillano H, Yin HL (1999). Gelsolin, a multifunctional actin regulatory protein. *J Biol Chem* 274(47), 33179–33182. doi: 10.1074/jbc.274.47.33179
- Sun X, Zhou Y, Zhang R, Wang Z, Xu M, Zhang D, Huang J, Luo F, Li F, Ni Z, et al. (2020). *Dstyk* mutation leads to congenital scoliosis-like vertebral malformations in zebrafish via dysregulated mTORC1/TFEB pathway. *Nat Commun* 11(1), 479. doi: 10.1038/s41467-019-14169-z
- Vassileva K, Marsh M, Patel S (2020). Two-pore channels as master regulators of membrane trafficking and endocytic well-being. *Curr Opin Physiol* 17, 163–168. doi: 10.1016/j.cophys.2020.08.002
- Wang X, Zhang X, Dong X, Samie M, Li X, Cheng X, Goschka A, Shen D, Zhou Y, Harlow J, et al. (2012). TPC Proteins are phosphoinositide-activated sodium-selective ion channels in

- endosomes and lysosomes. *Cell* 151(2), 372–383. doi: 10.1016/j.cell.2012.08.036
- Webb SE, Kelu JJ, Miller AL (2020). Role of two-pore channels in embryonic development and cellular differentiation. *Cold Spring Harb Perspect Biol* 12, a035170. doi: 10.1101/cshperspect.a035170
- Webb SE, Miller AL (2013). Microinjecting holo-aequorin into dechorionated and intact zebrafish embryos. *Cold Spring Harb Prot* 5, 447–455. doi: 10.1101/pdb.prot072967
- Westerfield M (2000). *The Zebrafish Book. A Guide for the Laboratory Use of Zebrafish (Danio rerio)*, 4th ed Eugene, USA: University of Oregon Press. https://zfin.org/zf_info/zfbook/zfbk.html
- Wickner W (2010). Membrane fusion: Five lipids, four SNARES, three chaperones, two nucleotides, and a Rab, all dancing in a ring on yeast vacuoles. *Annu Rev Cell Dev Biol* 26(1), 115–136. doi: 10.1146/annurev-cellbio-100109-104131
- Wöll S, Windoffer R, Leube RE (2005). Dissection of keratin dynamics: Different contributions of the actin and microtubule systems. *Eur J Cell Biol* 84(2–3), 311–328. doi: 10.1016/j.ejcb.2004.12.004
- Wopat S, Bagwell J, Sumigray KD, Dickson AL, Huitema LFA, Poss KD, Schulte-Merker S, Bagnat M (2018). Spine patterning is guided by segmentation of the notochord sheath. *Cell Rep* 22(8), 2026–2038. doi: 10.1016/j.celrep.2018.01.084
- Yamamoto M, Morita R, Mizoguchi T, Matsuo H, Isoda M, Ishitani T, Chitnis AB, Matsumoto K, Crump JG, Hozumi K, et al. (2010). Mib-Jag1-Notch signaling regulates patterning and structural roles of the notochord by controlling cell-fate decisions. *Development* 137(15), 2527–2537. doi: 10.1242/dev.051011
- Yasuoka Y (2020). Morphogenetic mechanisms forming the notochord rod: The turgor pressure-sheath strength model. *Develop Growth Differ* 62(6), 379–390. doi: 10.1111/dgd.12665
- Zhang C, Hicks GR, Raikhel NV (2014). Plant vacuole morphology and vacuolar trafficking. *Front Plant Sci* 5. doi: 10.3389/fpls.2014.00476
- Zhang J, Webb SE, Ma LH, Chan CM, Miller AL (2011). Necessary role for intracellular Ca²⁺ transients in initiating the apical-basolateral thinning of enveloping layer cells during the early blastula period of zebrafish development. *Develop Growth Differ* 53, 679–696. doi: 10.1111/j.1440-169X.2011.01275.x
- Zhou Y, Zhou B, Pache L, Chang M, Khodabakhshi AH, Tanaseichuk O, Benner C, Chanda SK (2019). Metascape provides a biologist-oriented resource for the analysis of systems-level datasets. *Nat Commun* 10(1), 1523. doi: 10.1038/s41467-019-09234-6